Supporting Information

Population of Exciton-Polaritons *via* Luminescent sp^3 Defects in Single-Walled Carbon Nanotubes

*Jan M. Lüttgens, Felix J. Berger, Jana Zaumseil**

Institute for Physical Chemistry and Centre for Advanced Materials, Universität Heidelberg, D-69120 Heidelberg, Germany

*zaumseil@uni-heidelberg.de

SWCNT film and dispersion characterization

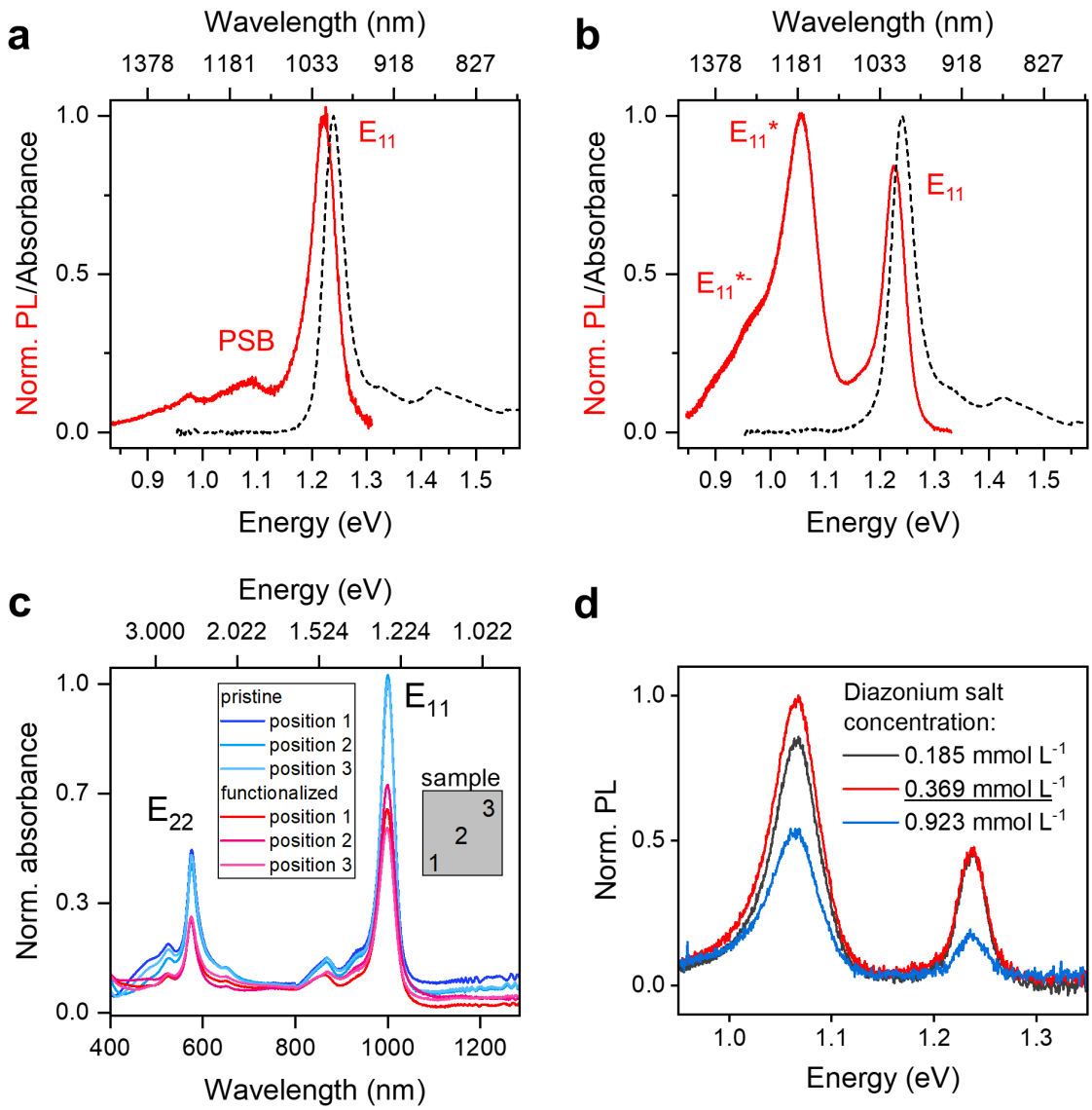

Figure S1. PL spectra (red solid line) of (a) pristine (normalized to E_{11}) and (b) functionalized (normalized to E_{11}*) (6,5) SWCNT films with PFO-BPy as the matrix polymer on glass. Absorbance spectra of both films are shown for reference (black dashed line). c) Absorbance spectra for the same films at three different sample positions corrected for film thickness and normalized to the E_{11} absorbance of the pristine SWCNTs. d) PL spectra of functionalized (6,5) SWCNT dispersions in toluene for three different diazonium salt concentrations. The spectra are normalized to the E_{11}* emission of the sample with 0.369 mmol L^{-1} (red) of diazonium salt in the reaction mixture, which was used for cavity fabrication in this study. Note that higher diazonium salt concentrations lead to a decrease in overall photoluminescence quantum yield (blue curve) as described in detail by Berger *et al.*[1]

Analysis of angle-integrated polariton emission spectra

Due to the geometric restrictions of the fluorescence mapping and TCSPC setup, the polariton emission cannot be angularly resolved and was collected confocally. The angle-integrated (confocal) PL measured with this setup (**Figure S2a**) agrees well with the sum over the angle-resolved PL from -30° to 30° (**Figure S2b**). Accordingly, the data in Figure 2 corresponds to an integration over these angles. For the fluorescence lifetime measurements, only emission at the wavelengths corresponding to $k_{||} = 0$ was collected. The maximum range of angles that contribute to this emission is ±20° for cavity detunings up to -33 meV based on the FWHM (full width at half maximum) (**Figures S2b and S2c**). Note that for detunings closer to resonance, the curvature around $k_{||} = 0$ decreases, leading to an increased contribution from larger angles.

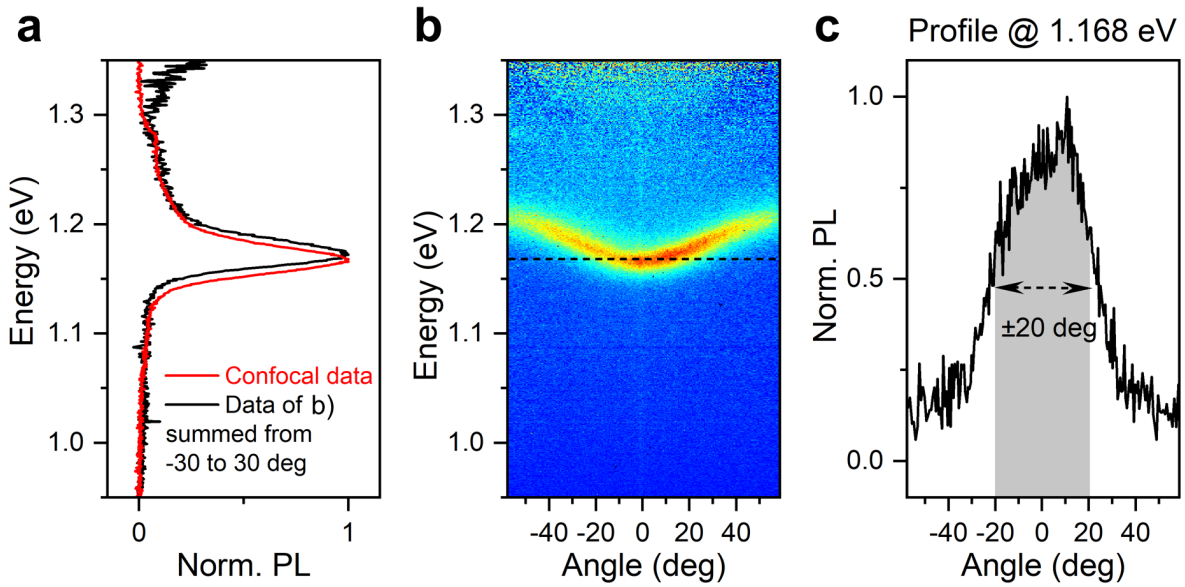

Figure S2. a) Normalized PL of the same sample measured confocally at a position with similar detuning (red line) and the sum of the data in (b) from −30° to 30° for comparison (black line). b) Angle-resolved PL of a SWCNT microcavity in the strong coupling regime c) Intensity profile of data in (b) at 1.168 eV.

Thickness determination by transfer matrix simulation

Spin-coated films exhibit inherent thickness gradients, which result in height differences of several tens of nanometers over a large sample area. The films prepared in this work varied by about 40 nm in thickness from the sample center to the edge. To account for this variation, we simulated the cavity reflectivity using transfer matrix simulations as described previously.[2]

The oxide spacer and gold mirror thicknesses can be assumed to be constant for one sample. All observed changes in the polariton modes are produced by the variation of the SWCNT layer thickness (assuming the absence of large defects or aggregates). Accordingly, the polariton mode position is indicative of the layer thickness. By simulating the reflectivity spectra for the employed SWCNT concentration for a given thickness, an area with the desired layer thickness can be identified on the sample by matching the lower polariton energetic position with that of the simulation.

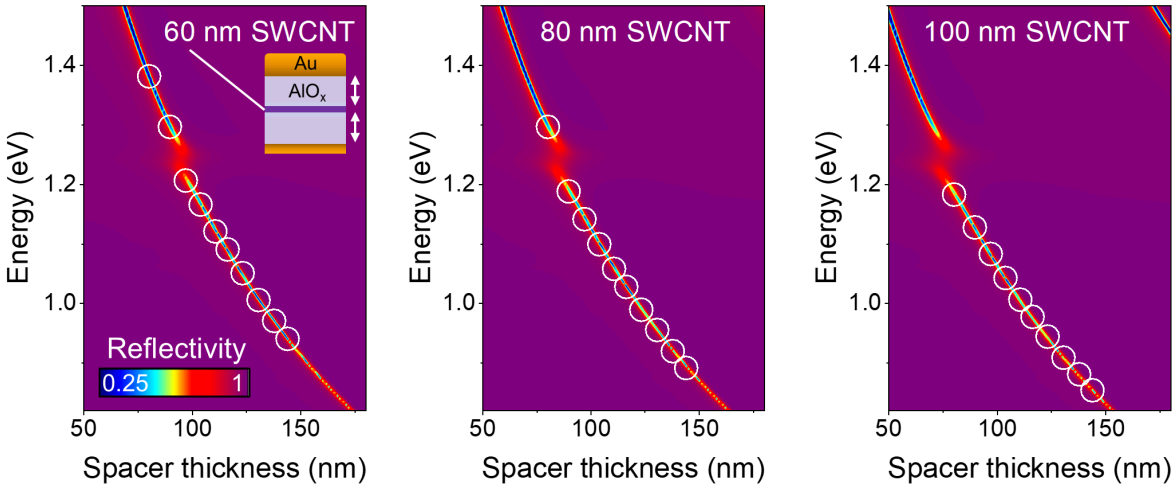

Figure S3. Transfer matrix simulations of the reflectivity of the cavity stack as a function of oxide spacer thickness for SWCNT films with 60, 80 and 100 nm thickness. The thickness of one oxide spacer is given on the x-axis. The cavity stack is shown as an inset. White circles indicate the polariton mode energy (UP for positive, LP for negative detunings) for 10 of the produced oxide spacer thicknesses.

Coupled oscillator fit results and angle-dependent spectra

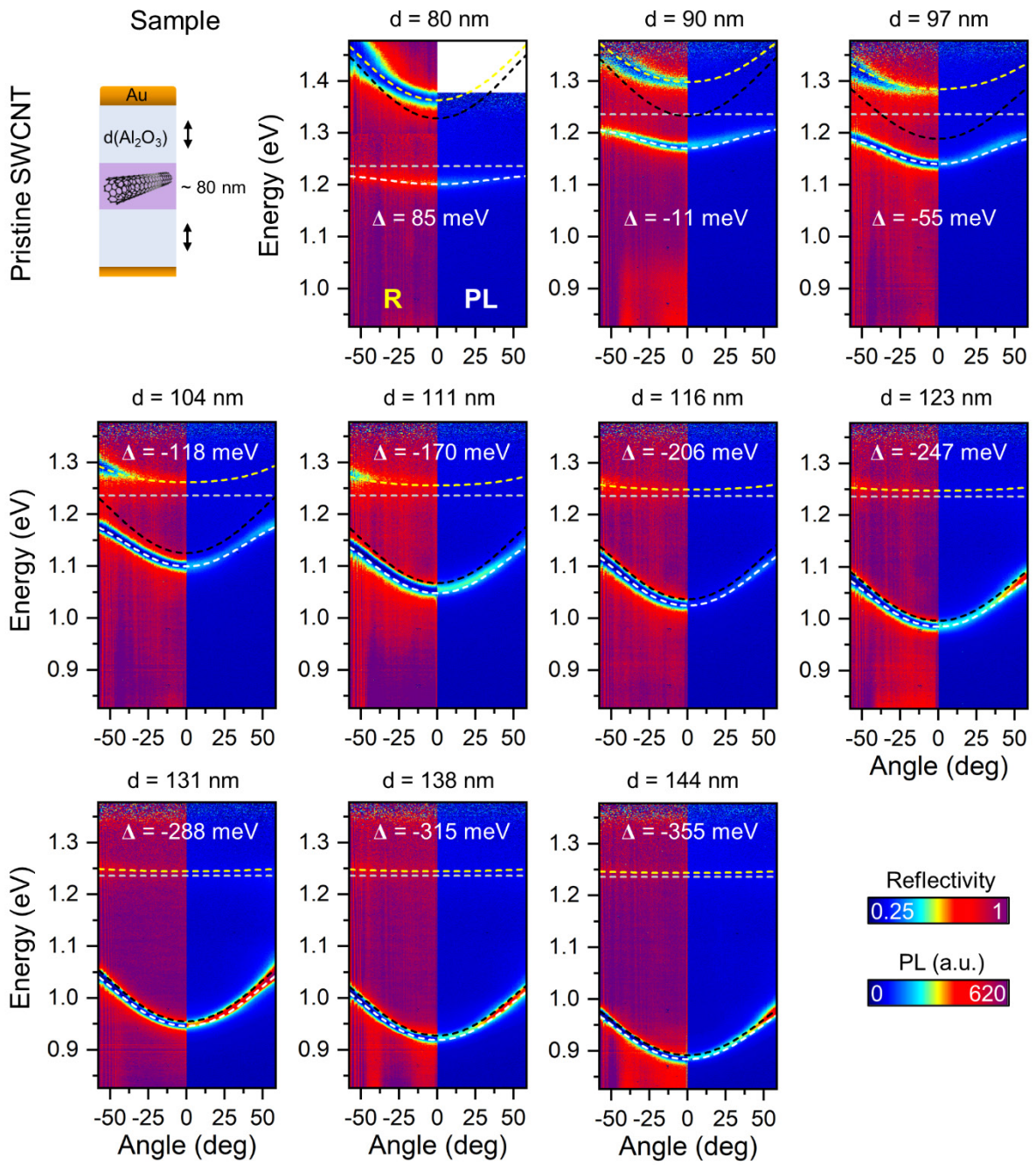

Figure S4. Angle-resolved reflectivity (R) and photoluminescence (PL) spectra for a cavity with an 80 nm thick film of pristine SWCNTs for different oxide spacer thicknesses. The fitted modes are given as dashed lines: UP (yellow), cavity (black) and LP (white). The energy of the E_{11} exciton is indicated by a dashed grey line. The oxide spacer thickness and the detuning obtained from the fits are presented for each data set. For the sample with 85 meV detuning, the upper polariton was recorded with a Si CCD camera (Princeton Instruments, PIXIS:400).

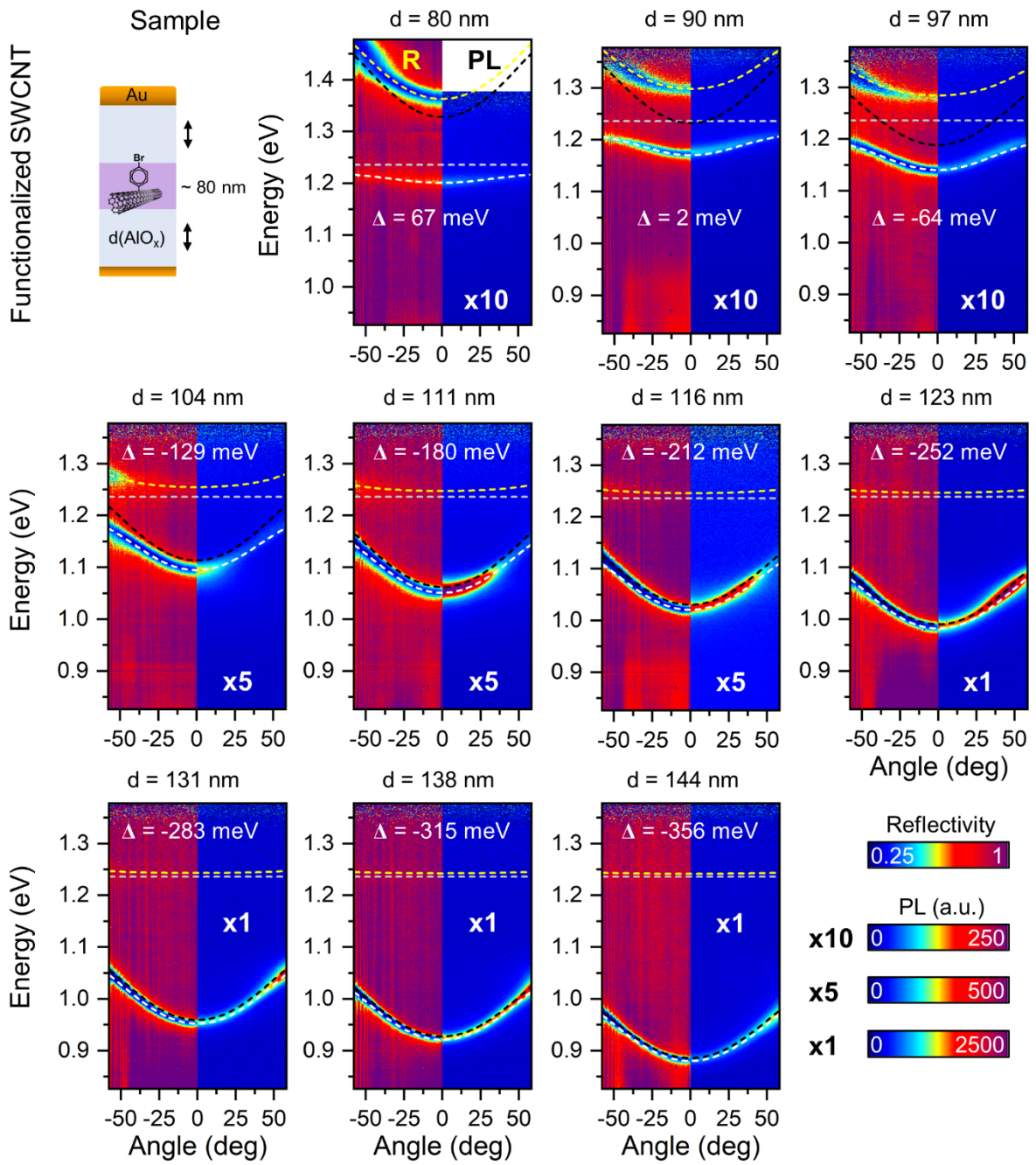

Figure S5. Angle-resolved reflectivity (R) and photoluminescence (PL) spectra for a cavity comprising an 80 nm thick film of functionalized SWCNTs for different oxide spacer thicknesses. The fitted modes are given as dashed lines: UP (yellow), cavity (black) and LP (white). The energy of the E_{11} exciton is indicated by a dashed grey line. The oxide spacer thickness and the detuning resulting from the fit are presented for each data set. For detunings of 67 meV to -212 meV the color scale was adapted to make the LP emission visible. For the sample with 67 meV detuning, the upper polariton was recorded with a Si CCD camera (Princeton Instruments, PIXIS:400).

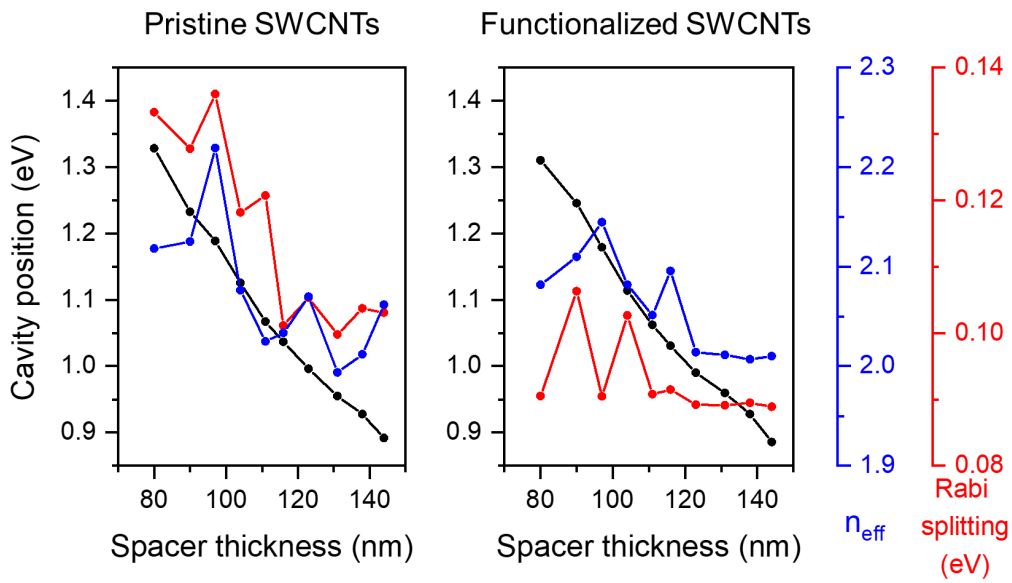

Figure S6. Results of coupled oscillator fits to the polariton modes recorded in reflectivity (TM polarization) for pristine and functionalized (6,5) SWCNTs. The results are sorted by spacer thickness of the cavity. The SWCNT layer thickness is always 80 nm. The fitted modes and the corresponding reflectivity data are shown in **Figure S4** and **S5**.

Cavity PLE spectra

Cavity photoluminescence-excitation (PLE) maps were recorded by focusing the spectrally filtered output of a picosecond-pulsed supercontinuum laser source (Fianium WhiteLase SC400, ~6 ps pulse width, 20 MHz repetition rate, ~20 μJ cm^{-2} pulse energy) through a ×100 nIR-optimized objective (N.A. 0.85, Olympus) onto the sample. The angle-integrated emission spectra were recorded for excitation wavelengths from 520 to 880 nm using a spectrograph (Acton SpectraPro SP2358) and an InGaAs line camera (Princeton Instruments OMA V). The recorded data was corrected for the wavelength dependence of the laser output power and the detection sensitivity.

Figure S7 shows the PLE maps for a microcavity with a pristine (a) and a functionalized (b) SWCNT layer. Both cavities are tuned to a PL transition around ~1130 nm, corresponding to X_1 in the case of the pristine SWCNT and to the blue flank of the E_{11}* in case of the functionalized SWCNT. For both samples the PLE emission maximum is observed at this wavelength. The emission maxima correlate with 575 nm and 860 nm in excitation, thus corresponding to the SWCNT E_{22} absorption peak and the phonon sideband of the E_{11} absorption, respectively. This correlation confirms that the origin of the cavity emission is the excitation of the (6,5) SWCNT at higher excited states for both the pristine and the functionalized SWCNT, respectively. The E_{11} emission in both cases is only faintly visible, resulting from a weakly coupled fraction of E_{11} excitons. This observation agrees well with a strongly coupled E_{11} transition. The lower intensity of the 860 nm excitation peak in comparison to the references (**Figures S7c** and **S7d**) is attributed to the onset of the gold mirror reflectivity. The lower intensity of the E_{11}* compared to the E_{11} transition in **Figure S7d** is due to the high peak power of the picosecond-pulsed laser, which already starts to saturate the E_{11}* transition.[1]

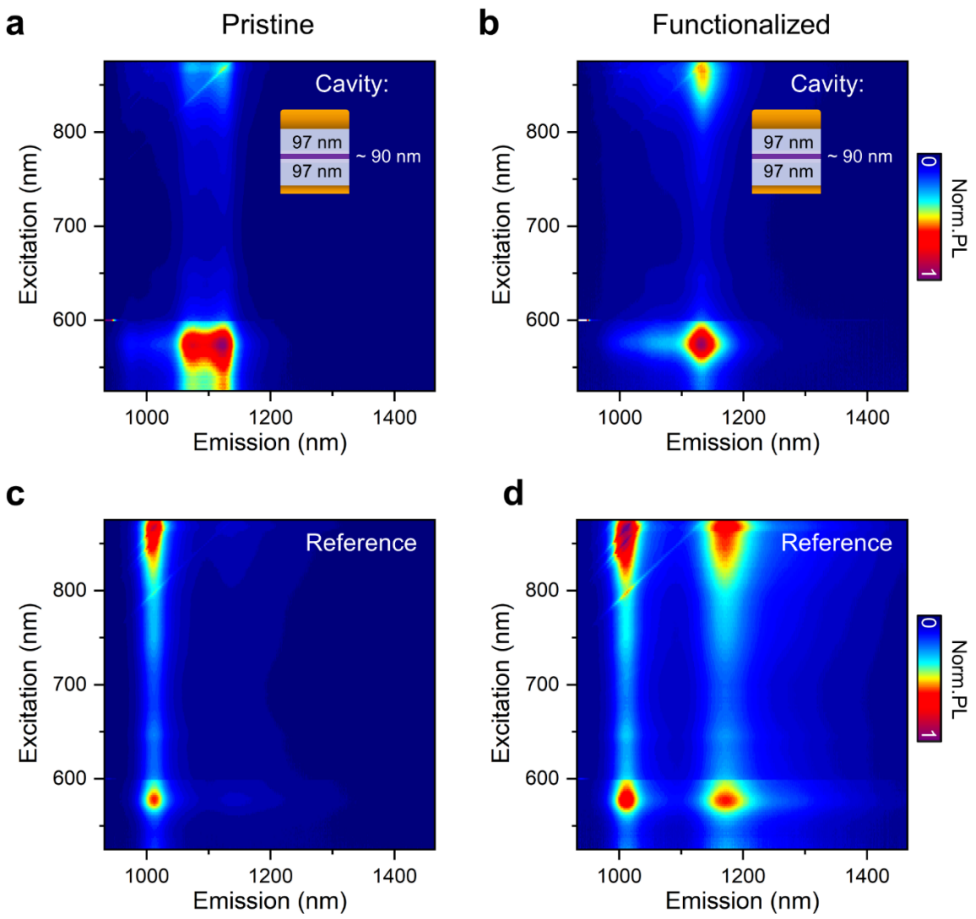

Figure S7. PLE maps of microcavities filled with pristine (a) and functionalized (b) SWCNT tuned to the X_1 and the E_{11}* transition, respectively, and the corresponding pristine (c) and functionalized (d) SWCNT reference films on glass. The cavity structure is shown in the inset. Note that the lower intensity of the E_{11}* compared to the E_{11} transition in (d) is due to the high peak power of the picosecond-pulsed laser, which already starts to saturate the E_{11}* defects.

Fluorescence lifetime measurements

The cavity fluorescence decay dynamics were investigated using time-correlated single photon counting (TCSPC). The sample was mounted onto a microscope stage and the excitation laser (575 nm, ~6 ps pulse width, 20 MHz repetition rate, ~20 μJ cm^{-2} pulse energy) was focused through a ×100 nIR-optimized objective (N.A. 0.85, Olympus). As described in the previous section, for each lifetime measurement an angle-integrated emission spectrum was recorded using a spectrograph (Acton SpectraPro SP2358) and an InGaAs line camera (Princeton Instruments OMA-V) to select the sample position of interest. The cavity emission wavelength at $k_{\parallel} = 0$ was selected and focused onto a gated InGaAs/InP avalanche photodiode (Micro Photon Devices) through a ×20 nIR-optimized objective (Mitutoyo). Statistics of the arrival times of the photons were acquired with a TCSPC module (Picoharp 300, Picoquant GmbH). The same procedure was used to measure the fluorescence decay of the pristine and functionalized SWCNT reference films of the respective PL bands. The instrument response function (IRF) was estimated for each sample from the fast, detector-limited PL decay of the (6,5) SWCNTs at the E_{11} transition at 1015 nm. All decay curves were fitted to a biexponential model in a reconvolution procedure correcting for the IRF. The detection limit based on the IRF FWHM of ~80 ps using this procedure was 8 ps.

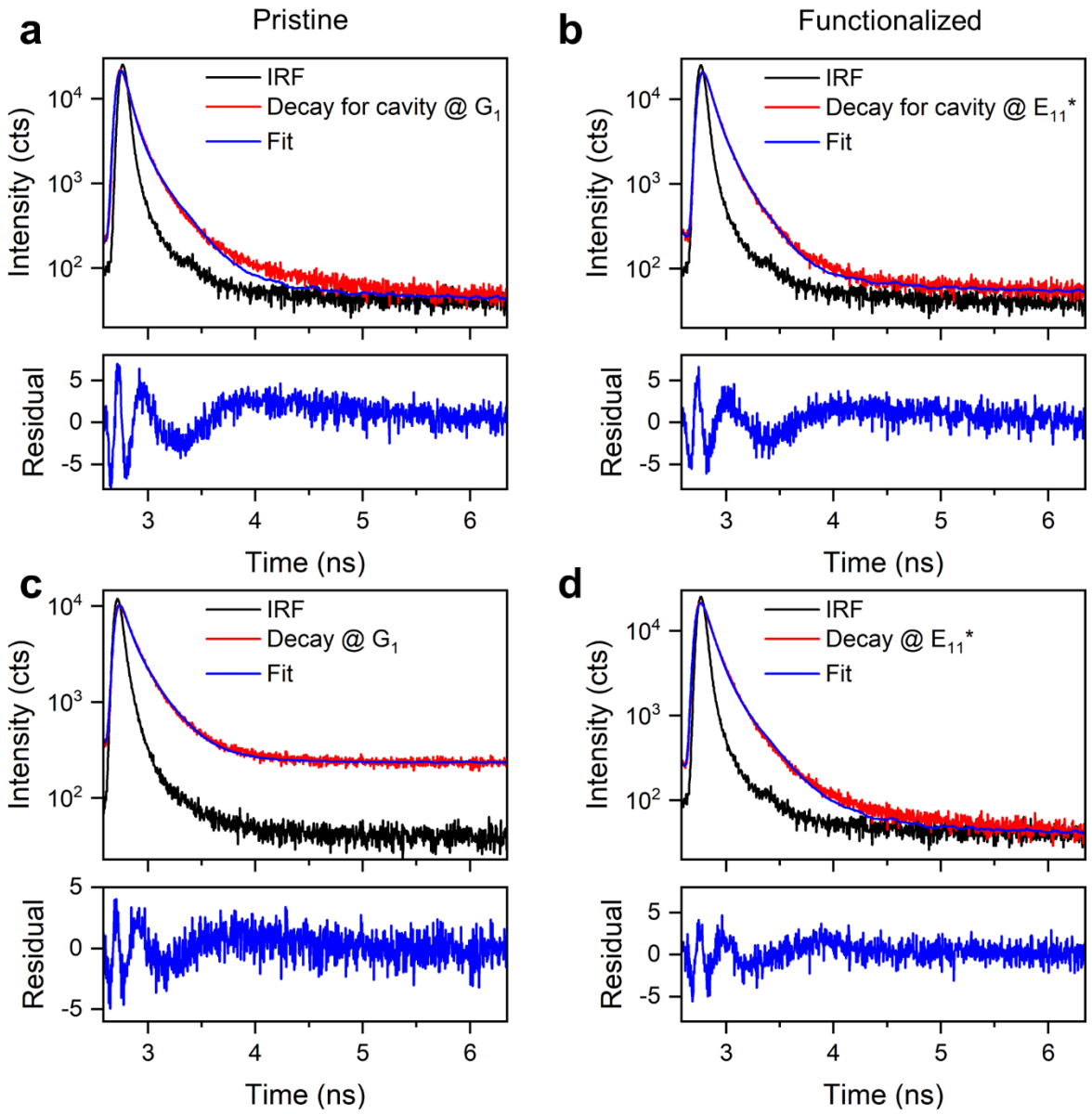

Figure S8. TCSPC histograms showing the fluorescence decay (red curve, upper plots) for a cavity with pristine SWCNTs tuned to the G_1 band (a), a cavity with functionalized SWCNTs tuned to the E_{11}* band (b). The respective decays of reference films on glass are depicted in (c) and (d). The biexponential fit (blue curve) was determined with a reconvolution procedure considering the IRF (black curve). Residuals of the respective fits to the decays are given in the lower plots. The spiking of the residual at early times results from the reconvolution.

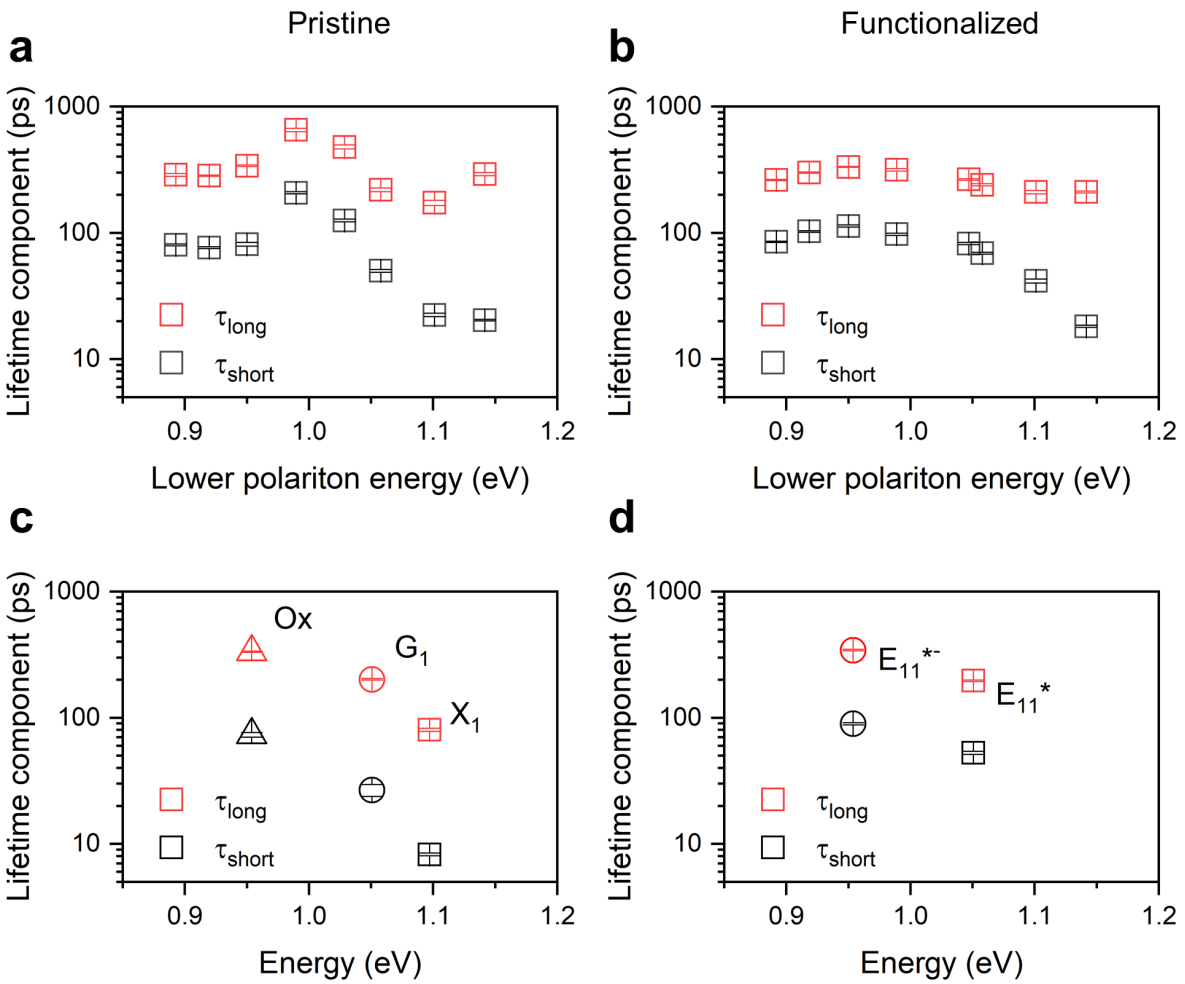

Figure S9. Long and short lifetime components of the cavity fluorescence decay as a function of lower polariton energy for pristine (a) and functionalized (b) SWCNTs. (c, d) Short and long lifetimes for the respective reference films as a function of emission energy. The error bars represent the error of the biexponential fit and reconvolution.

Estimate of mean exciton distance

For the lifetime measurements, samples were excited at 575 nm (E_{22} transition) with pulsed laser light (20 MHz, ~6 ps pulse width). The average laser power was ~100 µW corresponding to 1.4×10^{7} photons per pulse. The film absorbance at the E_{22} transition was determined to be ~0.15 for the pristine and ~0.1 for the functionalized samples, corresponding to an absorption of ~29 % and ~21 % of incident photons, respectively. For simplicity, we will use the average value in the following. The E_{22} to E_{11} conversion efficiency was estimated to be around 91 %.[3] However, complete conversion takes about 5 ps such that the generated E_{11} excitons can already diffuse to quenching sites or sp^3 defects.[4] We can estimate the fraction of freely diffusing excitons, that are not quenched or trapped, *via* the absolute PL quantum yield of the pristine film, which is around 0.2 %.[1] With this value we calculate $6.4\cdot10^{3}$ excitons per pulse. Considering that the beam was focused on a ~2 µm diameter spot and the presented lifetime data was recorded for an 80 nm thick SWCNT-polymer layer, the excited volume was about 10^{-12} cm^3. This yields an exciton density of $6.4\cdot10^{15}$ cm^{-3} per pulse. As the SWCNT are dispersed homogeneously in the polymer matrix, we can approximate the mean exciton distance with Wigner-Seitz radius yielding 155 nm. The error of the mean exciton distance mainly arises from the uncertainty of the laser pulse power and excitation spot diameter. It enters through the estimation of the exciton density. We estimate that the uncertainty in these quantities might lead to a variation of the rate by a factor of three at maximum.

Polariton fluorescence decay lifetime in the limit of VAS

We estimate the scattering rate W_{VAS} for vibrationally assisted scattering (VAS) in the adiabatic approximation by:[5]

$$W_{\mathrm{VAS}} = \left(\frac{a}{L_{\mathrm{c}}}\right)^3 \frac{\pi^2 g^2 (\Omega/2)^2 E_{\mathrm{c}}(k_0^2)}{\hbar E_c^2(0)} = 1/\tau_{\mathrm{VAS}}$$

We replace the mean distance between molecules (a) by the mean distance of excitons in the SWCNT, which we estimated to be 155 nm in the TCSPC experiments (see previous section). For metal cavity mirrors we can approximate the cavity length as $L_{\mathrm{c}} = \frac{\lambda_{\mathrm{res}}}{2n_{\mathrm{eff}}}$, where λ_{res} is the resonant wavelength and n_{eff} is the cavity effective refractive index. The dimensionless exciton-phonon coupling constant g was experimentally determined for the G phonon as 0.9.[6] Note that we neglect the radial breathing mode (RBM) here, as it is not able to transfer relative momentum.[7] The coupling constants for the remaining SWCNT optical phonons were determined theoretically and have comparable magnitudes to g_G.[7] For simplicity, we will assume the existence of an optical phonon for each investigated cavity detuning using g_G as the coupling constant. $E_c(0)$ is the cavity resonance at $k_{||} = 0$ and $E_{\mathrm{c}}(k_0^2)$ is the cavity energy for the position $k_{||} = k_0$, where the energy of the optically active phonon E_{vib} matches the energy difference $\Delta E = E_{\mathrm{X}} - E_{\mathrm{LP}}(k_0^2)$ between exciton reservoir and LP. All cavity parameters as well as the Rabi splitting $\hbar\Omega$, are taken from the coupled oscillator model fitted to the experimental angle-dependent reflectivity data of the respective sample. With these values we calculate $\tau_{\mathrm{VAS}} \approx 90 - 500$ fs depending on the cavity detuning. The results are shown in **Figure 5**. Given such a high scattering rate, we would expect the fluorescence decay to be detection limited.

Absence of Purcell effect and implications for radiative pumping

To understand the nature of the observed emission enhancement by radiative pumping, it is helpful to conduct the following thought experiment: As reported previously,[8-11] the exciton reservoir still undergoes decay processes as in the weak coupling regime because only a small fraction of excitons (1-30 %)[12] is coherently coupled to the light field. The polariton modes rather represent additional states, into which the reservoir population can decay. Starting from this, we consider a radiative transition of the exciton reservoir to the ground state and the resulting photon as weakly coupled. Secondly, we consider the photonic part of the polariton modes as electromagnetic modes in the classical sense. If the polariton is tuned to the energy of the photon, this should lead to Purcell enhancement of the underlying transition. For the condition that the SWCNT layer lies at the anti-node of the electric field created by the polariton (**Figure S10**), we can estimate the Purcell factor $F_P^{2\mathrm{D}}$ by:[13, 14]

$$F_P^{2\mathrm{D}} = \frac{1}{4\pi}\frac{\lambda_{\mathrm{res}}}{n_{\mathrm{eff}}L_{\mathrm{c}}}Q$$

where the resonant wavelength is λ_{res} (1.1 meV), here tuned to X_1 (1.092 meV). The cavity effective refractive index n_{eff} (2.08) and the quality factor of Q_{exp} (44.9) were taken from the experimental reflectivity data of a strongly-coupled microcavity with pristine SWCNT tuned to X_1 (**Figure S4**, Δ = – 118 meV). The cavity length L_{c} is $\frac{\lambda_{\mathrm{res}}}{2n_{\mathrm{eff}}} = 271$ nm (see **Figure S10**). With these values we calculate $F_P^{2\mathrm{D}} = 7.2$. This Purcell factor is equivalent to a sevenfold decrease of the radiative lifetime in the cavity compared to free space. Such a considerable increase of the radiative decay should be observable in the fluorescence decay. Note that the non-radiative decay is not altered by the cavity, accordingly any enhancement due to the Purcell effect must also affect the fluorescence lifetime. If the enhancement of the radiative decay is small compared to the intrinsic non-radiative decay, also no significant increase of the LP

emission should be observable. **Figure S11** shows TCSPC time traces of a cavity with pristine and functionalized SWCNTs and their respective reference films measured at the same energy. Note that no change of fluorescence lifetime is found. So far, we could not measure Purcell enhancement for any of our strongly coupled cavities. Based on this observation, we consider the weakly coupled photons as being absorbed by the polaritons and the resulting emission as polaritonic. In a potential fluorescence up-conversion experiment (currently not available) the fluorescence decay of the reference should be faster than that of the polaritons, as the photons will remain within the sample for the duration of the lifetime of the polaritons.

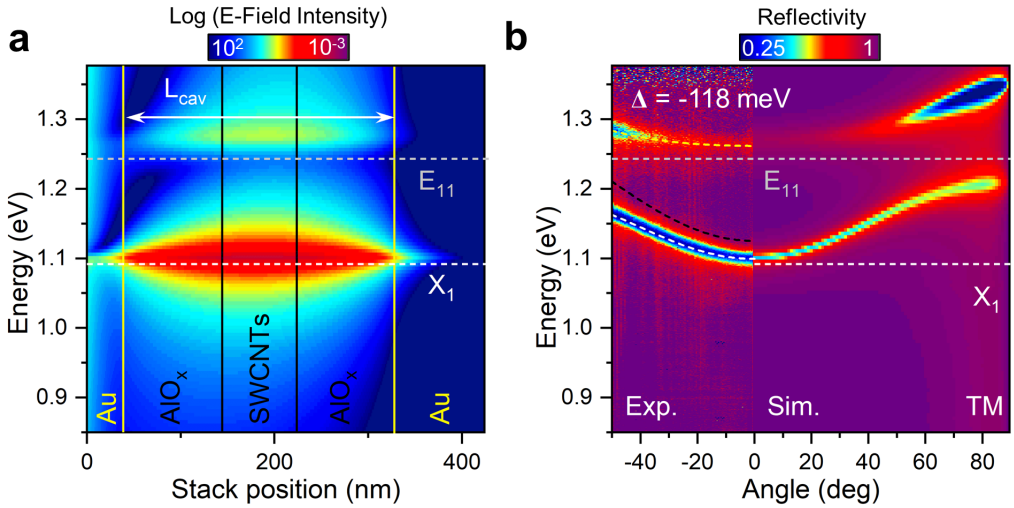

Figure S10. (a) Electric field intensity of the photonic part of the polariton at $k_{\|} = 0$ in the microcavity of **Figure S4** ($\Delta = -118$ meV) from transfer matrix calculations. The different materials of the device stack and the relevant transitions of pristine SWCNTs are indicated. (b) Experimental and simulated angle-dependent reflectivity of the same sample. The photon fraction of the LP at $k_{\|} = 0$ is 85 % (based on coupled oscillator fit to experimental reflectivity).

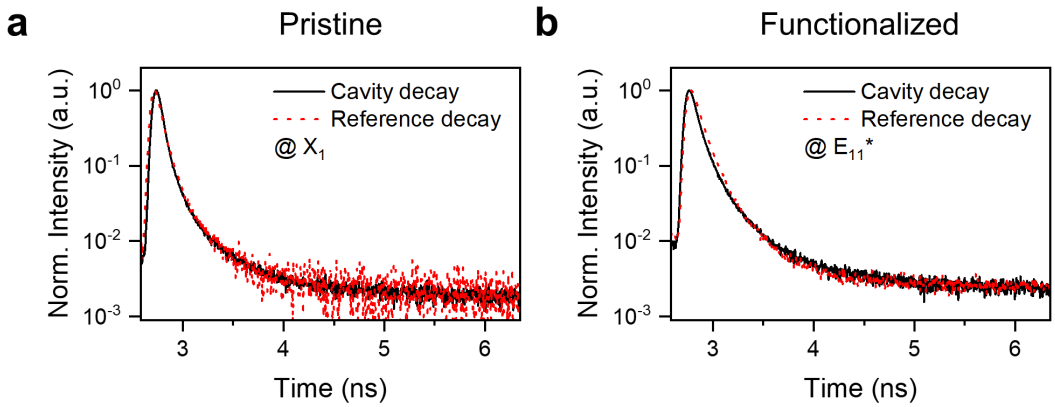

Figure S11. Fluorescence decay of pristine (at X_1 emission) and functionalized (at E_{11}* emission) SWCNTs in a cavity and for a reference film.

Polariton emission at $k_{\|} = 0$ as a function of detuning

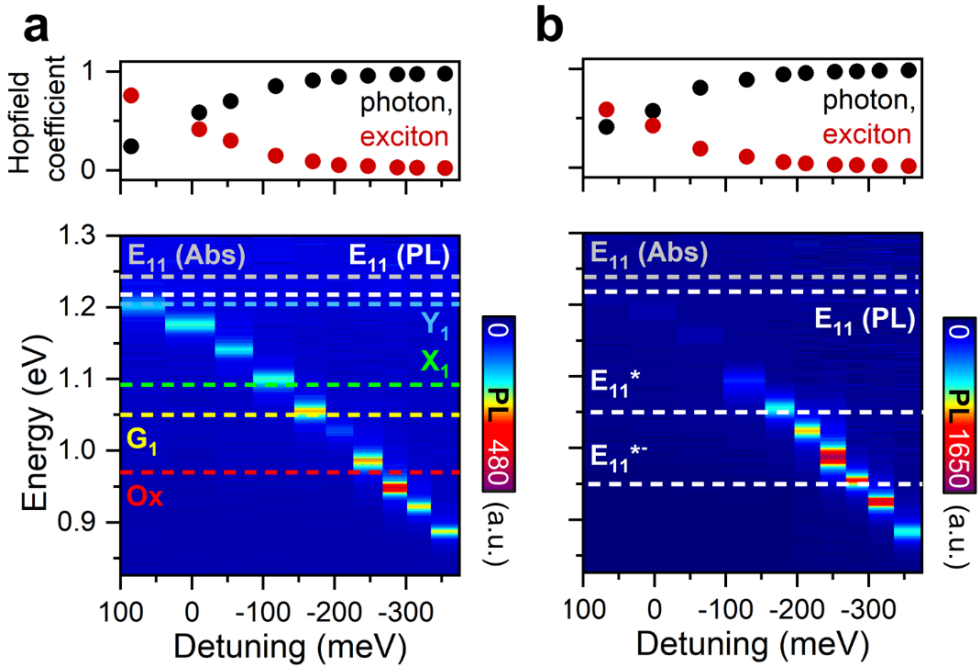

Figure S12. Emission intensities of the LP at $k_{\|} = 0$ as a function of detuning for (a) a microcavity filled with pristine SWCNTs, and (b) a microcavity filled with functionalized SWCNTs. The corresponding Hopfield coefficients of the LP for excitons (red dots) and photons (black dots) are given for comparison. The respective photoluminescence sidebands and sp^3 defects are indicated as dashed lines for comparison. For cavities tuned around 0.98 eV the λ mode overlaps with the excitation wavelength (640 nm).

Excitation efficiency correction for population analysis

To account for the change in excitation efficiency for the different cavities, we simulated the electric field intensity within each structure for the employed excitation wavelength of 640 nm. Since the laser linewidth (±2 nm) is small compared to the cavity resonance (±9 nm), we can neglect its spectral shape. To calculate the electric field, we used the transfer matrix method as described in Ref. 2. Firstly, we matched the mode positions of the experimental reflectivity data by adjusting the SWCNT thickness and holding the metal mirror and oxide spacer thicknesses fixed. With the obtained thicknesses we simulated the electric field and calculated the overlap with the SWCNT layer (**Figures S13**). The resulting overlaps were normalized to the smallest field overlap (1.83) to obtain the correction factors (**Figure S14**). The correction factors were multiplied with the populations of the different samples according to their spacer thickness.

We estimated the uncertainties added by correcting the population data (**Figure 6**) as follows. The highest uncertainty of the simulation input is the SWCNT layer thickness, which is given by the standard deviation of the layer thicknesses used to match the experimental data, that is, 1.8 nm. This uncertainty leads to an error in the LP position of the population data, because the correction factors are mapped using the spacer thickness (th_{Spacer}). Additionally, close to the λ mode, even a small change in SWCNT layer thickness affects the excitation efficiency and hence the population strongly. To account for both, we weighted the standard deviation of the SWCNT layer thickness (th_{SWNCT}) with the slope of a Bézier interpolation of the correction factors (**Figure S14**).

$$\Delta(th_{SWCNT}) = STD(th_{SWCNT}) \cdot \left(1 + 100 \cdot \left|\frac{\partial \text{BézierInterpol.}}{\partial th_{Spacer}}\right|\right)$$

We converted this uncertainty to the uncertainty in LP position as follows: Firstly, we calculated the optical cavity length (th_{cav}) in TM polarization for the strongly coupled λ/2 mode (the refractive indices n can be assumed constant for the considered spectral range).

$$th_{cav} = \left(th_{SWCNT} \cdot 2 \cdot n_{SWCNT,TM}\right) + \left(th_{spacer} \cdot 4 \cdot n_{Spacer,TM}\right)$$

Secondly, we calculated the respective error, that results from the uncertainty in SWCNT thickness

$$\Delta th_{cav} = \left(\Delta th_{SWCNT} \cdot 2 \cdot n_{SWCNT,TM}\right)$$

Using error propagation, we converted the uncertainty of the cavity thickness into energy.

$$\Delta th_{cav}[eV] = \left(hc/{th_{cav}}^2\right) \cdot \Delta th_{cav}$$

We assume Δth_{cav} to be a good measure for the error of the LP position given in **Figure 6**.

Additionally, the correction factor itself should have an uncertainty due to the previously made approximations. The error should scale with the magnitude of the correction factor. However, this error can only be estimated heuristically. We chose it to be the difference of each correction factor to a B-spline interpolation of the correction factors (**Figure S14**). Together with the standard deviation for averaging over ±1.5° around $k_{\|} = 0$, this yielded the error in population shown in **Figure 6**.

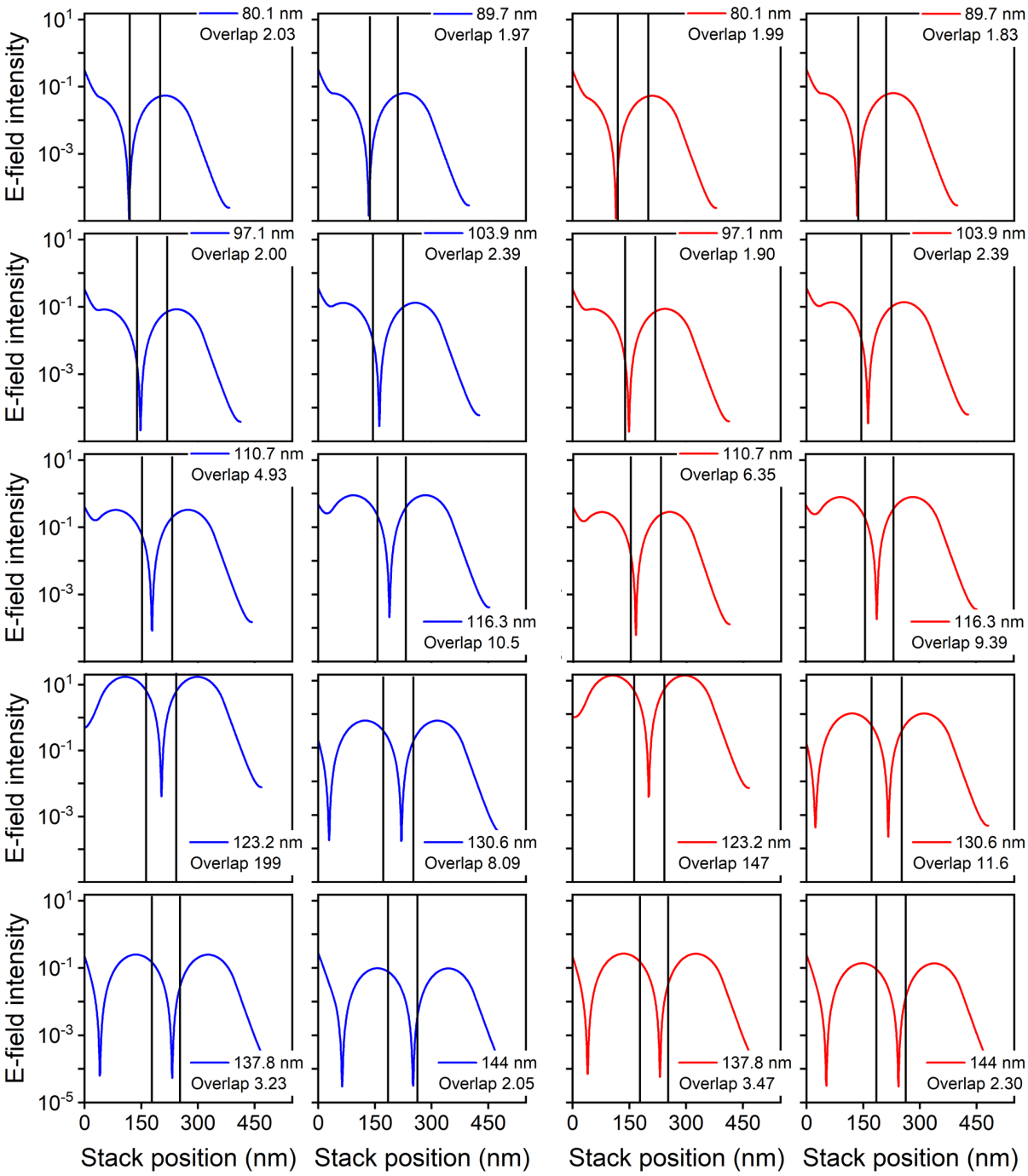

Figure S13. Transfer matrix simulation of the electric field intensity as a function of stack position for cavities with pristine (blue) and functionalized SWCNTs (red). The position of the SWCNT layer is indicated by black solid lines. The overlap was calculated as the integral of the electric field intensity within the SWCNT layer.

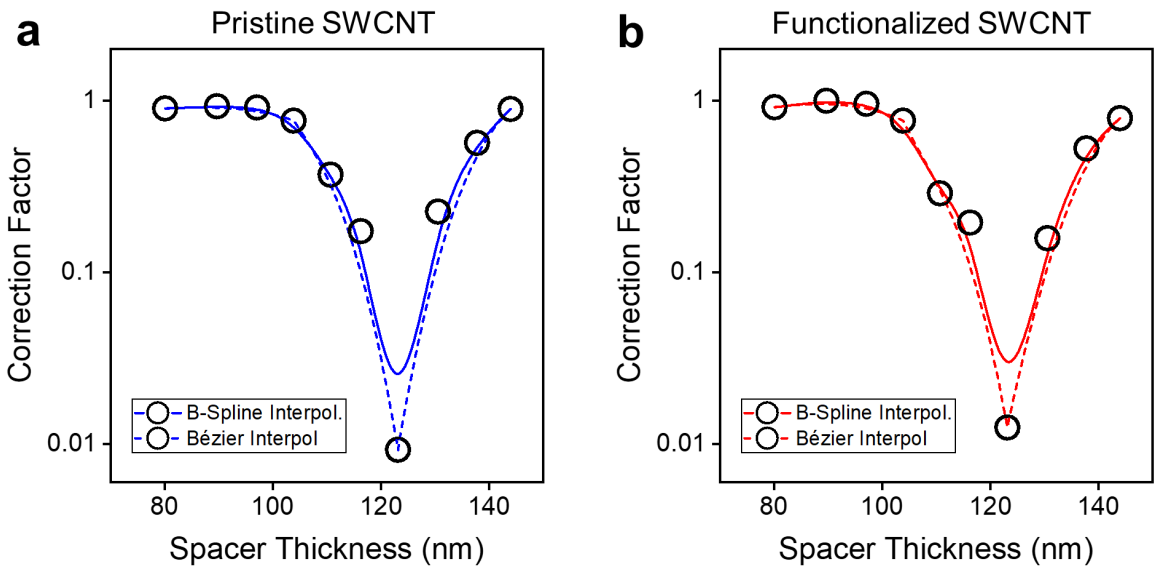

Figure S14. Excitation efficiency correction factors for cavities with pristine (a) and functionalized SWCNTs (b). To estimate the error of the correction, the factors were interpolated with a B-spline (solid lines) and a Bézier curve (dashed lines). The highest population reduction is obtained for the cavity detuning at which the λ mode is in resonance with the laser excitation wavelength.

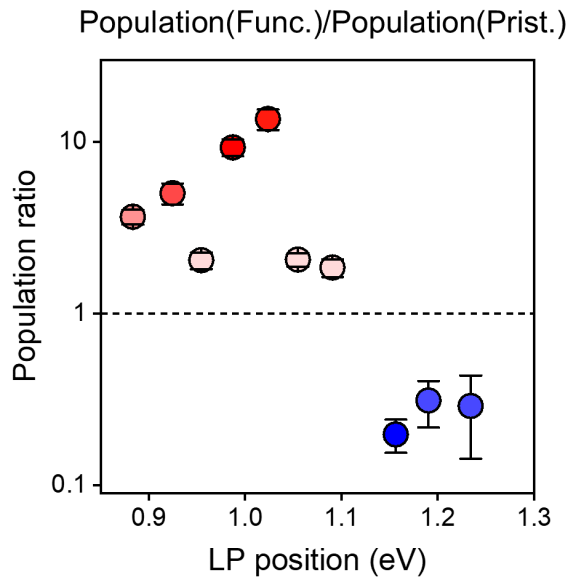

Figure S15. Population ratio of the LP population for cavities with functionalized SWCNTs divided by the LP population for cavities with pristine SWCNTs as a function of LP position. The color code is given as in **Figure 6** for comparison.

LP population as a function of defect emission

To test how the LP population changes with the number of occupied sp^3-defect states, we recorded the power dependence of the PL emission of a cavity tuned to the E_{11}* transition and the PL emission of a functionalized (6,5) SWCNT reference film. Note that the E_{11}* emission saturates earlier with pump power than the E_{11} emission for functionalized SWCNTs as previously described by Berger *et al.*[1]

To excite the SWCNT layer of both samples with the same power, we accounted for the power loss at the top mirror by measuring the transmission of the excitation source (640 nm laser diode, Coherent OBIS, continuous wave) through a 25 nm gold reference film. The result was extrapolated to the 40 nm top mirror thickness using Beer's law. With this correction we estimated the power loss to be 95 % at 640 nm for the top mirror. We collected the angle-dependent polariton PL and the PL of the reference film at the corresponding excitation powers, the data is shown in **Figure S16a** and **S16b**. After fitting the reflectivity spectrum of the polaritons using the coupled oscillator model we corrected the LP emission at $k_{||} = 0$ for the LP fraction to extract the polariton population. The E_{11}* emission intensity was obtained by taking the peak area (**Figure S16b**, shaded area) and subtracting the noise level. For the investigated excitation powers, the LP population at $k_{||} = 0$ shows a nearly linear dependence on the E_{11}* emission intensity. Hence, we attribute the change in polariton population directly to the change in E_{11}* emission, which further confirms the radiative pumping mechanism.

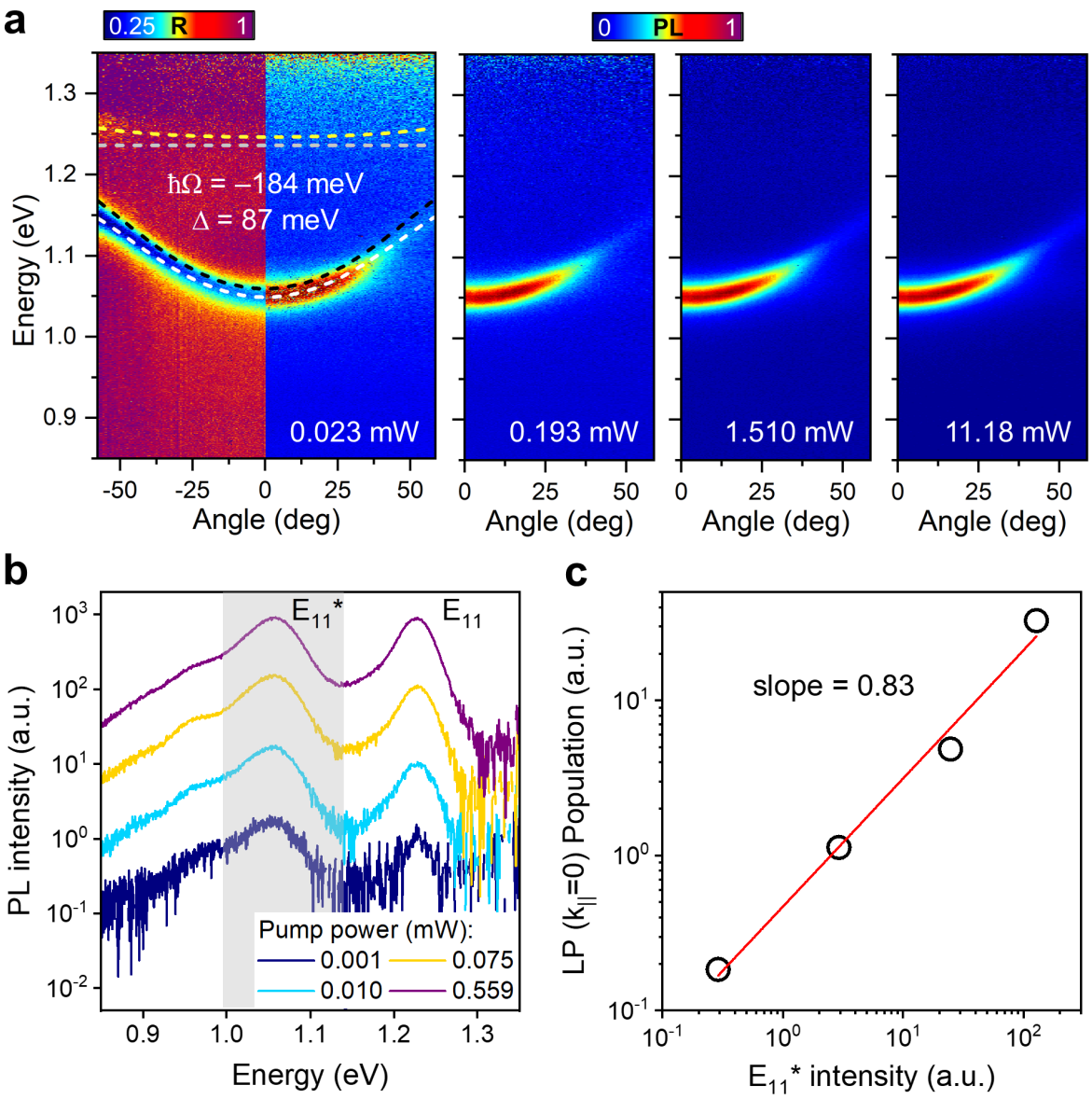

Figure S16. (a) Angle-dependent reflectivity and normalized PL spectra for a metal-clad cavity with functionalized SWCNTs tuned to the E_{11}* transition. The PL spectra are shown for four different excitation powers. (b) PL spectra of a functionalized SWCNT reference film for four equivalent excitation powers with regard to the cavity PL given in (a) (corresponding to 95 % power loss at the top mirror). (c) LP population at $k_{\|} = 0$ given in (a) as a function of the E_{11}* emission intensity given in (b) for four equivalent excitation powers. The film thickness of the functionalized SWCNT layer was about 80 nm for the cavity and reference.

REFERENCES

(1) Berger, F. J.; Lüttgens, J.; Nowack, T.; Kutsch, T.; Lindenthal, S.; Kistner, L.; Müller, C. C.; Bongartz, L. M.; Lumsargis, V. A.; Zakharko, Y.; Zaumseil, J., Brightening of Long, Polymer-Wrapped Carbon Nanotubes by Sp3 Functionalization in Organic Solvents. *ACS Nano* **2019,** *13*, 9259-9269. doi: 10.1021/acsnano.9b03792

(2) Graf, A.; Tropf, L.; Zakharko, Y.; Zaumseil, J.; Gather, M. C., Near-Infrared Exciton-Polaritons in Strongly Coupled Single-Walled Carbon Nanotube Microcavities. *Nat. Commun.* **2016,** *7*, 13078. doi: 10.1038/ncomms13078

(3) Hertel, T.; Perebeinos, V.; Crochet, J.; Arnold, K.; Kappes, M.; Avouris, P., Intersubband Decay of 1-D Exciton Resonances in Carbon Nanotubes. *Nano Lett.* **2008,** *8*, 87-91. doi: 10.1021/nl0720915

(4) Harrah, D. M.; Schneck, J. R.; Green, A. A.; Hersam, M. C.; Ziegler, L. D.; Swan, A. K., Intensity-Dependent Exciton Dynamics of (6,5) Single-Walled Carbon Nanotubes: Momentum Selection Rules, Diffusion, and Nonlinear Interactions. *ACS Nano* **2011,** *5*, 9898-9906. doi: 10.1021/nn203604v

(5) Litinskaya, M.; Reineker, P.; Agranovich, V. M., Fast Polariton Relaxation in Strongly Coupled Organic Microcavities. *J. Lumines.* **2004,** *110*, 364-372. doi: 10.1016/j.jlumin.2004.08.033

(6) Lüer, L.; Gadermaier, C.; Crochet, J.; Hertel, T.; Brida, D.; Lanzani, G., Coherent Phonon Dynamics in Semiconducting Carbon Nanotubes: A Quantitative Study of Electron-Phonon Coupling. *Phys. Rev. Lett.* **2009,** *102*, 127401. doi: 10.1103/PhysRevLett.102.127401

(7) Popov, V. N.; Lambin, P., Intraband Electron-Phonon Scattering in Single-Walled Carbon Nanotubes. *Phys. Rev. B.* **2006,** *74*, 075415. doi: 10.1103/PhysRevB.74.075415

(8) Grant, R. T.; Michetti, P.; Musser, A. J.; Gregoire, P.; Virgili, T.; Vella, E.; Cavazzini, M.; Georgiou, K.; Galeotti, F.; Clark, C.; Clark, J.; Silva, C.; Lidzey, D. G., Efficient Radiative Pumping of Polaritons in a Strongly Coupled Microcavity by a Fluorescent Molecular Dye. *Adv. Opt. Mater.* **2016,** *4*, 1615–1623 doi: 10.1002/adom.201600337

(9) Lidzey, D. G.; Fox, A. M.; Rahn, M. D.; Skolnick, M. S.; Agranovich, V. M.; Walker, S., Experimental Study of Light Emission from Strongly Coupled Organic Semiconductor Microcavities Following Nonresonant Laser Excitation. *Phys. Rev. B* **2002,** *65*, 195312. doi: 10.1103/PhysRevB.65.195312

(10) Coles, D. M.; Michetti, P.; Clark, C.; Tsoi, W. C.; Adawi, A. M.; Kim, J.-S.; Lidzey, D. G., Vibrationally Assisted Polariton-Relaxation Processes in Strongly Coupled Organic-Semiconductor Microcavities. *Adv. Funct. Mater.* **2011,** *21*, 3691-3696. doi: 10.1002/adfm.201100756

(11) Virgili, T.; Coles, D.; Adawi, A. M.; Clark, C.; Michetti, P.; Rajendran, S. K.; Brida, D.; Polli, D.; Cerullo, G.; Lidzey, D. G., Ultrafast Polariton Relaxation Dynamics in an Organic Semiconductor Microcavity. *Phys. Rev. B: Condens. Matter* **2011,** *83*, 245309. doi: 10.1103/PhysRevB.83.245309

(12) Litinskaya, M.; Reineker, P.; Agranovich, V. M., Exciton–Polaritons in Organic Microcavities. *J. Lumin.* **2006,** *119-120*, 277-282. doi: 10.1016/j.jlumin.2006.01.016

(13) Kavokin, A.; Baumberg, J. J.; Malpuech, G.; Laussy, F. P., *Microcavities*. 2007; p 429.

(14) Genco, A.; Giordano, G.; Carallo, S.; Accorsi, G.; Duan, Y.; Gambino, S.; Mazzeo, M., High Quality Factor Microcavity Oled Employing Metal-Free Electrically Active Bragg Mirrors. *Org. Electron.* **2018,** *62*, 174-180. doi: 10.1016/j.orgel.2018.07.034